sciendo

CAIM
ISSN 2038-0909

Commun. Appl. Ind. Math. 11 (1), 2020, 55–71 DOI: 10.1515/caim-2020-0004

Research Article

A new two-component approach in modeling red blood cells

Luca Meacci[1*], Gustavo C. Buscaglia[1], Fernando Mut[2], Roberto F. Ausas[1], Mario Primicerio[3,4]

[1]Instituto de Ciências Matemáticas e de Computação, ICMC, Universidade de São Paulo, São Carlos (SP), Brazil

[2]Bioengineering Department, George Mason University, Fairfax (VA), USA

[3]Dipartimento di Matematica "U. Dini", Università degli Studi di Firenze, Firenze, Italy

[4]Istituto per le Applicazioni del Calcolo "M. Picone", CNR, Roma, Italy

[*]Email address for correspondence: luca.meacci@usp.br

Communicated by Giorgio Fotia

Received on 06 16, 2020. Accepted on 09 14, 2020.

Abstract

This work consists in the presentation of a computational modelling approach to study normal and pathological behavior of red blood cells in slow transient processes that can not be accompanied by pure particle methods (which require very small time steps). The basic model, inspired by the best models currently available, considers the cytoskeleton as a discrete non-linear elastic structure. The novelty of the proposed work is to couple this skeleton with continuum models instead of the more common discrete models (molecular dynamics, particle methods) of the lipid bilayer. The interaction of the solid cytoskeleton with the bilayer, which is a two-dimensional fluid, will be done through adhesion forces adapting efficient solid-solid adhesion algorithms. The continuous treatment of the fluid parts is well justified by scale arguments and leads to much more stable and precise numerical problems when, as is the case, the size of the molecules ($0.3\,nm$) is much smaller than the overall size ($\simeq 8000\,nm$). In this paper we display some numerical simulations that show how our approach can describe the interaction of an RBC with an exogenous body as well as the relaxation of the shape of an RBC toward its equilibrium configuration in absence of external forces.

Keywords: `Red blood cell, Mathematical modeling, Biological fluid mechanics, Lipid membrane, cytoskeleton, Fluid-solid interactions, Cell biology`

AMS subject classification: `76Zxx, 74F10, 74L15, 92Cxx`

1. Introduction

Red blood cells (RBC) occupy between 35 and 50 % of the total blood volume in the human circulatory system. Their mechanical characteristics are highly relevant for the biological functions of blood, not only because they have direct consequences in hemodynamics [1,2] but also because the way RBC respond (e.g., to shear stress) may impact the synthesis of nitric oxide and thus the regulation of vascular tonus [3].

In human blood, a RBC (or erythrocyte) has the shape of a biconcave disk, flattened and depressed in the centre, with a cross-section of dumbbell shape [4]. In its undeformed state, the discoid has a diameter of $6-8\,\mu m$ and its average thickness is $2\,\mu m$. Typical erythrocytes have a volume of $90\,\mu m^3$ and a surface area of $136\,\mu m^2$ (see e.g. [5]). Therefore, while in blood vessels with a diameter larger than $200\,\mu m$ (like arteries) the flow of the blood can be modeled in terms of a homogeneous non-newtonian fluid, when we consider the circulation in vessels whose internal diameter is comparable with the size of RBCs (arterioles, venules, and capillaries) it becomes essential to consider the blood as a suspension of erythrocytes and to take into account their morphological evolution.

Indeed, blood can flow in capillaries with diameter smaller than that of RBCs, because RBCs change their shape from the original biconcave one to that of a bullet or of a parachute and then recover their initial state. Therefore modeling erythrocytes is essential for an appropriate description of the blood flow and its functions in microcirculation [6]. Analogous situations are frequent: as long as it is possible to apply a continuum approach by averaging the relevant quantities over a small volume the available

methods are relatively simple and well established [7]; however, sometimes intrinsic heterogeneities become fundamental because different components react differently to the same external stimulus [8]. In those cases even a single-cell approach can be instrumental for modeling the system or for developing therapeutic strategies [9]. The present paper aims to contribute under this regard.

A human RBC is a nucleus-free cell whose basic mechanical structure consists of a cytoskeleton formed by a spectrin network and of a fluid-like lipid bilayer. In what concerns Mechanics, lipid bilayers are two-molecule-thick sheets of phospholipid molecules which are known to function as osmotic barriers with viscous tangential behavior and bending resistance. The spectrin network is like an internal reinforcement thought to play a role in the stability of the RBC's shape [10]. The spectrin network attaches, through a *junction complex* (JC), to proteins that are "floating" in the bilayer among the (much smaller) lipid particles. The JCs can be associated to nodes of a network of fibers with elastic or viscoelastic behavior. The attachment of the JCs to the bilayer is strong enough for them to remain attached in most physiological conditions, but under extreme conditions it is known that detachment occurs before the bilayer itself breaks [11].

In [12,13] a computational scheme was presented in which both the bilayer and the cytoskeleton are modeled as a discrete system of interacting particles. This requires particles describing the behavior of the lipid molecules, of the spectrin fibers, of the JCs, and also possibly of the inner and outer three-dimensional liquids. More precisely, the cytoskeleton is described as a set of JCs (nodes) connected by nonlinear springs obeying a worm-like-chain law (other laws have also been considered [14]). The typical length of the spectrin filaments is about 70 nanometers, which corresponds to a number of about $30,000$ nodes for the cytoskeleton. This number is small enough for the numerical simulation of the complete cytoskeleton to be feasible. For certain studies that require low-cost solvers, some coarse graining rules are available that allow to reduce the number of nodes by a factor of 10 or 100 without significant loss in physical accuracy [14].

The use of particles to describe the lipid bilayer, on the other hand, is more questionable. The number of molecules in the bilayer is about 700 million, so that each of the numerical particles must model thousands or tens of thousands of molecules for the cumputing cost to be affordable.

Taking these facts into account, we adopt the following strategy: maintaining the discrete description of the cytoskeleton as in [12,13], we model the lipid bilayer in terms of a continuous surface fluid. In particular, we adopt the viscous liquid shell model with Canham-Helfrich bending energy described by Arroyo et al. [15], with a discretization based on the method of Rodrigues et al. [16] that has sufficient generality to accomplish this task. The two sub-systems are coupled by adhesion forces that bind the cytoskeleton and the bilayer, inspired by the computational contact formulations for soft body adhesion of Sauer [17].

In this paper we describe the model and display some numerical simulations in specific situations that show how our approach is promising in view of future applications. In particular, we consider a case of interaction with an exogenous body, and the relaxation of an RBC from a deformed configuration towards its equilibrium state, in absence of external forces.

2. Mathematical formulation

We consider a red blood cell as a mechanical system whose configuration is described by the state $\mathcal{X}$ of the cytoskeleton and the state $\mathcal{Y}$ of the lipid bilayer. In Figure 1 we show a scheme of a RBC depicting the two components of the model. The configuration $\mathcal{X}$ represents a state of the cytoskeleton, which in our model is a set of N_X balls of radius R representing the junctional complexes of the cytoskeleton. In this way, appropriate coordinates for $\mathcal{X}$ are the positions of the *nodes* of the cytoskeleton model, which are the centers of the aforementioned balls. These coordinates will be denoted by $\{\mathbf{X}^j\}_{j=1}^{N_X}$. Consequently, the instantaneous motion of the cytoskeleton nodes are described by $\mathbf{U}^j = \frac{d\mathbf{X}^j}{dt}$.

Similarly, $\mathcal{Y}$ is a configuration of the lipid bilayer, which in the exact problem is an element of an infinite-dimensional manifold of possible membrane shapes of fixed volume and surface area. For numerical purposes, however, we parameterize the configuration $\mathcal{Y}$ by the positions of N_Y points, the *nodes* of the

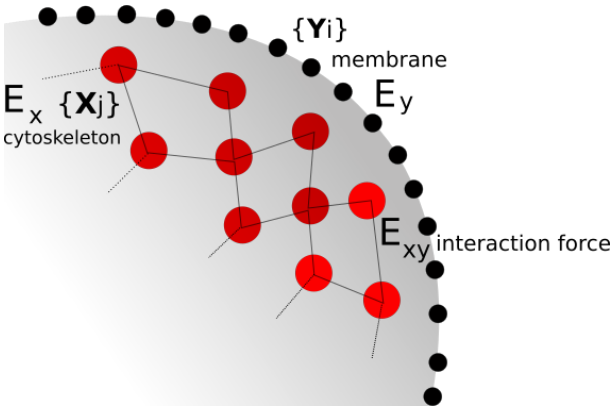

Figure 1. Skecth of the problem.

bilayer model. The coordinates of any configuration $\mathcal{Y}$ are thus $\{\mathbf{Y}^i\}_{i=1}^{N_Y}$. From these coordinates the *geometrical position* of the bilayer,

$$\Gamma(\mathcal{Y}) = \{\mathbf{y} \in \mathbb{R}^3 \mid \mathbf{y} \text{ belongs to the bilayer surface } \}\ , \tag{1}$$

can be reconstructed. The instantaneous motion of the bilayer particles is characterized by the rates of change of $\mathcal{Y}$,

$$\mathcal{W} = \frac{d\mathcal{Y}}{dt}\ . \tag{2}$$

This means that the tracking of the surface is *Lagrangian*. The discrete velocity $\mathbf{w}$, evaluated at the i-th bilayer node, coincides with that of the lipid particle at $\mathbf{Y}^i(t)$(i.e., $\mathbf{w}^i = \frac{d\mathbf{Y}^i}{dt}$). In this latter sentence "lipid particle" is to be understood not as a lipid molecule but as a small macroscopic chunk of lipid material, in the spirit of Continuum Mechanics.

The energy $\mathcal{E}$ of the proposed two-component system (that clearly depends on $\mathcal{X}$ and $\mathcal{Y}$) is decomposed into the sum

$$\mathcal{E}(\mathcal{X},\mathcal{Y}) = \mathcal{E}_X(\mathcal{X}) + \mathcal{E}_Y(\mathcal{Y}) + \mathcal{E}_{XY}(\mathcal{X},\mathcal{Y}) \tag{3}$$

where $\mathcal{E}_X$ is the intrinsic skeleton energy, $\mathcal{E}_Y$ the intrinsic bilayer energy, and $\mathcal{E}_{XY}$ the interaction energy between the cytoskeleton and the bilayer.

We consider as starting point for the mathematical formulation of the problem the **principle of virtual work** demanding that the virtual change in energy of the system for an admissible virtual variation of the configuration variables plus the work done by the dissipative forces equals the work done by the external forces [18]. The corresponding expression can be formally written as

$$d_X\mathcal{E}(\mathcal{X},\mathcal{Y}) \bullet \delta\mathcal{X} + d_Y\mathcal{E}(\mathcal{X},\mathcal{Y}) \bullet \delta\mathcal{Y} + \mathcal{D}(\mathcal{X},\mathcal{Y},\mathcal{U},\mathcal{W}) \bullet (\delta\mathcal{X},\delta\mathcal{Y}) = \mathcal{F}_X \bullet \delta\mathcal{X} + \mathcal{F}_Y \bullet \delta\mathcal{Y} \tag{4}$$

where

- $d_X\mathcal{E}(\mathcal{X},\mathcal{Y}) \bullet \delta\mathcal{X}$ is the infinitesimal change $\delta\mathcal{E}$, when the state of the system is perturbed from $(\mathcal{X},\mathcal{Y})$ to $(\mathcal{X}+\delta\mathcal{X},\mathcal{Y})$,
- the bullet $\bullet$ is an appropriate duality product which will take on meaning based on the single component model as presented below,
- $d_Y\mathcal{E}(\mathcal{X},\mathcal{Y}) \bullet \delta\mathcal{Y}$ is the infinitesimal change $\delta\mathcal{E}$, when the state of the system is perturbed from $(\mathcal{X},\mathcal{Y})$ to $(\mathcal{X},\mathcal{Y}+\delta\mathcal{Y})$,
- $\mathcal{D}(\mathcal{X},\mathcal{Y},\mathcal{U},\mathcal{W}) \bullet (\delta\mathcal{X},\delta\mathcal{Y})$ is the dissipation of the system (i.e., the work of its internal dissipative forces), when the system is perturbed by $(\delta\mathcal{X},\delta\mathcal{Y})$, and,
- the right-hand side is the virtual work of external forces.

Explicit expressions for the terms in (4) are derived from the mathematical modeling of each of the two components (bilayer, cytoskeleton) of the system, and of their interaction, as briefly introduced below.

2.1. *Lipid bilayer model*

Being Γ the average surface of the bilayer at time t, let H be the *average curvature* of Γ, $\check{\mathbf{n}}$ the normal vector and $\boldsymbol{\kappa}$ the *mean curvature vector*, defined as $\boldsymbol{\kappa} = H\,\check{\mathbf{n}}$. We also need the tangential projector $\mathbb{P} = \mathbb{I} - \check{\mathbf{n}} \otimes \check{\mathbf{n}}$. The *tangential gradient* ∇_Γ is the operator defined as $\nabla_\Gamma f = \mathbb{P}\,\nabla \widehat{f}$, where $f : \Gamma \to \mathbb{R}$ is any function and $\widehat{f}$ an arbitrary extension of f to an open neighborhood of $\Gamma \subset \mathbb{R}^3$. The constraints of constant volume and constant surface are imposed by means of Lagrange multipliers, namely a uniform pressure difference p and a space-dependent surface tension field σ, respectively.

Together with these definitions, we assume linear viscous dynamics of the lipid bilayer [15,19] and the Canham-Helfrich bilayer energy given by [20–22]

$$\mathcal{E}_Y = \frac{C_{ch}}{2} \int_\Gamma \|\boldsymbol{\kappa}\|^2 \,. \tag{5}$$

Then we can compute the part $\mathcal{D}_Y$ of the virtual dissipation that is intrinsic to the bilayer ($\delta\mathcal{X} = 0$, $\delta\mathcal{Y} = \mathbf{v}$) as

$$\mathcal{D}_Y \bullet \mathbf{v} = \int_\Gamma 2\,\mu\, D_\Gamma \mathbf{w} : D_\Gamma \mathbf{v} \,, \tag{6}$$

where μ is the *surface* viscosity, and the virtual change in energy as

$$d_Y \mathcal{E}_Y \bullet \mathbf{v} = C_{ch} \int_\Gamma \left[(\mathbb{I} - 2\,\mathbb{P}) \nabla_\Gamma \boldsymbol{\kappa} : \nabla_\Gamma \mathbf{v} + \frac{1}{2} (\nabla_\Gamma \cdot \boldsymbol{\kappa})\, (\nabla_\Gamma \cdot \mathbf{v}) \right] \,. \tag{7}$$

We need a few more definitions to completely define the mathematical model of the bilayer. The first two of them are the experimentally observed constraints of *isochoricity* (constant volume, enforced by osmotic pressure) and *inextensibility* (constant area of each bilayer parcel). These constraints are enforced through the Lagrange multipliers p (internal pressure) and σ (surface tension, a scalar field on Γ). Notice that, as any Lagrange multiplier, p and σ are unknowns of the problem and thus depend on the configuration of the bilayer and on the force applied on it. The last needed definition is that of the *interaction force field*, $\mathbf{f}^\Gamma$, that represents in an L^2 sense all the interaction terms in (4), i.e.

$$d_Y \mathcal{E}_{XY} \bullet \mathbf{v} + \mathcal{D}_{XY} \bullet \mathbf{v} = -\int_\Gamma \mathbf{f}^\Gamma \cdot \mathbf{v} \,. \tag{8}$$

In this way, the bilayer mathematical problem, assumed the interaction force $\mathbf{f}^\Gamma$ known for the moment, reads: *Find the unique fields* $\mathbf{w}$, σ, $\boldsymbol{\kappa}$ *and the only* $p \in \mathbb{R}$ *such that*

$$\begin{aligned} &\int_\Gamma 2\,\mu\, D_\Gamma \mathbf{w} : D_\Gamma \mathbf{v} \;- p \int_\Gamma \mathbf{v} \cdot \check{\mathbf{n}} \;+\; \int_\Gamma \sigma\, \nabla_\Gamma \cdot \mathbf{v} \;+ \\ &+ c_{CH} \int_\Gamma \left[(\mathbb{I} - 2\,\mathbb{P}) \nabla_\Gamma \boldsymbol{\kappa} : \nabla_\Gamma \mathbf{v} + \frac{1}{2} (\nabla_\Gamma \cdot \boldsymbol{\kappa})\, (\nabla_\Gamma \cdot \mathbf{v}) \right] = \int_\Gamma \mathbf{f}^\Gamma \cdot \mathbf{v} \end{aligned} \tag{9}$$

$$\int_\Gamma \xi\, \nabla_\Gamma \cdot \mathbf{w} = 0 \tag{10}$$

$$\int_\Gamma \boldsymbol{\kappa} \cdot \boldsymbol{\zeta} = \int_\Gamma \mathbb{P} : \nabla_\Gamma \boldsymbol{\zeta} \tag{11}$$

$$\int_\Gamma \mathbf{w} \cdot \check{\mathbf{n}} = 0 \tag{12}$$

$\forall\, (\mathbf{v}, \xi, \boldsymbol{\zeta}) \in \mathbf{V} \times Q \times \mathbf{K}$, where $\mathbf{V}$ and $\mathbf{K}$ are essentially $(H^1(\Gamma))^3$ and $Q = L^2(\Gamma)$. The equation (11) corresponds the weak form of the Laplace-Beltrami identity, while (10) and (12) are the constraints of fixed surface area and volume, respectively.

The methodology to solve this part of the bi-component model arises from the discretization of the above variational problem in space and in time. This has already been developed and published [23]. It incorporates automatic adjustment of the time step and surface remeshing [24]. The theoretical framework comes from the works by Dziuk, Elliot, and others [25–28].

In this contribution we incorporate the interaction with the cytoskeleton, as shown in Section 2.3 below. For that purpose, we first introduce in Section 2.2 the model for the internal skeletal component of the RBC.

2.2. *Cytoskeleton model*

The cytoskeleton will be treated by trying to follow the nature of its components, basically a spectrin fiber network with special joints [29]. The model considers a mesh made of a set of nodes (junctions) joined by molecular chains represented by worm-like chains [30–32]. The number of the elements of the skeleton is large ($\sim 10^5$) but numerically tractable. Also, coarse-grained models are available in the literature to save computing effort [33].

According to these premises, the elastic spectrin mesh energy $\mathcal{E}_X$ is defined as follows

$$\mathcal{E}_X = \sum_j \left[\frac{k_B T \ell_m \,(3x_j^2 - 2x_j^3)}{4\ell_p(1-x_j)} + \frac{k_p}{(n-1)\ell_j^{n-1}} \right] \tag{13}$$

where ℓ_j is the filament length j, ℓ_m is the maximum extension of these filaments, $x_j = \ell_j/\ell_m$, ℓ_p is the persistence length, k_BT is the unit of energy and n and k_p are parameters. A homogenized version of this model corresponds to an elastic shell of shear modulus [32]

$$G_0 = \frac{\sqrt{3}\, k_B T}{4\ell_p \ell_m x_0} \left(\frac{x_0}{2(1-x_0)^3} - \frac{1}{4(1-x_0)^2} + \frac{1}{4} \right) + \frac{\sqrt{3} k_p (n+1)}{4\,\ell_0^{n+1}} \tag{14}$$

with ℓ_0 the equilibrium spacing and $x_0 = \ell_0/\ell_m$, but, as said, our formulation keeps the worm-like chains without homogenizing them. The virtual change in energy is readily obtained by differentiating (13) with respect the vector of nodal coordinates. In this way, if no intrinsic dissipation is attributed to the cytoskeleton, if the interaction force on the j-th node is denoted by $\mathbf{F}^j$ and if m denotes the effective mass of each node, the equations governing the cytoskeleton movement are

$$m\,\frac{d^2\mathbf{X}^j}{dt^2} + \frac{\partial \mathcal{E}_X}{\partial \mathbf{X}^j} = \mathbf{F}^j \ . \tag{15}$$

The inertia is very small at the scale of the junction complexes, so that in this contribution we adopt $m = 0$. These equations are numerically integrated with an implicit Newmark scheme, which is well established in solid mechanics.

2.3. *Interaction Model*

The interaction between the bilayer and the cytoskeleton is modeled as adhesion of soft bodies, adapting the formulation of Sauer [17] based on the models and available data [11,34–36]. Denoting by Υ *the adherent surface* of the cytoskeleton, the contact energy, here denoted with $\mathcal{E}_{XY}$, takes the general form

$$\mathcal{E}_{XY} = \int_\Gamma \int_\Upsilon \beta_\Gamma \ \beta_\Upsilon \ \phi(\|\mathbf{x}^\Gamma - \mathbf{x}^\Upsilon\|) \ d\mathbf{x}^\Gamma \ d\mathbf{x}^\Upsilon \tag{16}$$

where ϕ is the potential of interaction (in Joule/m^4) and β_Γ, β_Υ are dimensionless scalars. One popular choice for ϕ is the Lennard-Jones (LJ) potential [37], i.e.,

$$\phi(d) = \varepsilon \left(\frac{r_0}{d}\right)^k - 2\varepsilon \left(\frac{r_0}{d}\right)^{k/2}, \tag{17}$$

where d is the distance between two particles and, r_0 and ε are length and energy scales, respectively. This potential has a minimum of value $-\varepsilon$ at $d = r_0$, it is repulsive for $d < r_0$ and attractive if $d > r_0$.

The force on the bilayer resulting from this energy, to be substituted in the right-hand side of (9), is

$$\mathbf{f}^{\,\mathrm{con},\Gamma}(\mathbf{x}^\Gamma) = -\,\beta_\Gamma \int_\Upsilon \beta_\Upsilon \phi'(\|\mathbf{x}^\Gamma - \mathbf{x}^\Upsilon\|)\, \frac{\mathbf{x}^\Gamma - \mathbf{x}^\Upsilon}{\|\mathbf{x}^\Gamma - \mathbf{x}^\Upsilon\|}\, d\mathbf{x}^\Upsilon \ . \tag{18}$$

Attributing a spherical shape of radius R and center $\mathbf{c}$ to Υ, this integral can be computed analytically as an explicit function $\mathcal{G}(\|\mathbf{x}^\Gamma - \mathbf{c}\| - R, r_0, \varepsilon)$ times the unit vector along $\mathbf{x}^\Gamma - \mathbf{c}$. The function $\mathcal{G}$ diverges when $d = \|\mathbf{x}^\Gamma - \mathbf{c}\| - R$ tends to 0, since $d < 0$ implies interpenetration. Such singularity is too difficult to deal with numerically. Instead, we regularize the model replacing it by

$$\widetilde{\mathcal{G}}(d, r_0, \varepsilon) = \begin{cases} \mathcal{G}(d, r_0, \varepsilon) & \text{if } \ d \geq z, \\ \mathcal{G}(z, r_0, \varepsilon) + \frac{\partial \mathcal{G}}{\partial d}(z, r_0, \varepsilon)\,(d - z) & \text{otherwise.} \end{cases} \tag{19}$$

The function $\widetilde{\mathcal{G}}$ is defined for all $d \in \mathbb{R}$, thus allowing a softer contact with some interpenetration. The parameter z is taken as αr_0, with $0 < \alpha < 1$. A typical value es $\alpha = 0.9$.

Similarly, the force exerted on a point x^Υ of the adherent surface of the cytoskeleton by the bilayer Γ is given by

$$\mathbf{f}^{\,\mathrm{con},\Upsilon}(\mathbf{x}^\Upsilon) = \beta_\Upsilon \int_\Gamma \beta_\Gamma \phi'(\|\mathbf{x}^\Gamma - \mathbf{x}^\Upsilon\|)\, \frac{\mathbf{x}^\Gamma - \mathbf{x}^\Upsilon}{\|\mathbf{x}^\Gamma - \mathbf{x}^\Upsilon\|}\, d\mathbf{x}^\Gamma \ . \tag{20}$$

It is immediate to see that $\int_\Gamma \mathbf{f}^{\,\mathrm{con},\Gamma} + \int_\Upsilon \mathbf{f}^{\,\mathrm{con},\Upsilon} = 0$, as expected from the action-reaction principle (see [38] for more details). The contact force only acts along the surface normal, it is complemented by a drag force that models the tangential attachment of the citoskeleton nodes to the bilayer anchoring proteins as

$$\mathbf{f}^{d,\Gamma}(\mathbf{x}^\Gamma) = -\int_\Upsilon \eta \left(\mathbf{w}(\mathbf{x}^\Gamma) - \frac{d\mathbf{x}^\Upsilon}{dt}\right) d\mathbf{x}^\Upsilon, \qquad \mathbf{f}^{d,\Upsilon}(\mathbf{x}^\Upsilon) = \int_\Gamma \eta \left(\mathbf{w}(\mathbf{x}^\Gamma) - \frac{d\mathbf{x}^\Upsilon}{dt}\right) d\mathbf{x}^\Gamma, \tag{21}$$

where η is a drag coefficient that depends on $\|\mathbf{x}^\Gamma - \mathbf{x}^\Upsilon\|$. We remark that, in the case of the cytoskeleton, the set $\{\mathbf{X}^i\}_{i=1}^{N_X}$ refers to the coordinates of the centers of the nodes, while Υ consists of spheres Υ^j of a given radius around $\mathbf{X}^j$, i.e., the surfaces of the junctions. The net force per unit area acting on the bilayer is thus $\mathbf{f}^\Gamma = \mathbf{f}^{\,\mathrm{con},\Gamma} + \mathbf{f}^{d,\Gamma}$, while the net force on node j, to be equilibrated by the worm-like chains (and possibly external forces) is

$$\mathbf{F}^j = \int_{\Upsilon^j} \left(\mathbf{f}^{\,\mathrm{con},\Upsilon}(\mathbf{x}^\Upsilon) + \mathbf{f}^{\,d,\Upsilon}(\mathbf{x}^\Upsilon)\right) d\mathbf{x}^\Upsilon \ . \tag{22}$$

In Figure 2 we plot the contact part of $\mathbf{F}$ (i.e., taking $\eta = 0$) and of $\mathcal{E}_{XY}$ as a function of d for a node of radius $R = 0.07$ in the vicinity of a typical biconcave surface (fixed). The maximum (positive) value of the force corresponds to the maximum *adhesion force* of the node to the surface. Notice that it takes place at $d \simeq r_0$. Similarly, the minimum value of the interaction energy corresponds to the *adhesion energy* and its position to the equilibrium distance. The regularization is evident in the repulsion forces, which depend approximately linearly with d for d much smaller than r_0.

2.4. *Model summary*

The main unknowns of the proposed **two-component RBC model (2C-RBC-M)** are the bilayer configurations $\Gamma(t)$ and the junctions' positions $\mathbf{X}(t)$, which evolve according to the instantaneous velocity field $\mathbf{w}(t)$ and nodal-velocity vector $\mathbf{U}(t)$, respectively. At each instant t, the system (9)-(12) coupled to (15) determine $\mathbf{w}$ and $\mathbf{U}$ (remember that we are assuming $m = 0$ for simplicity). The coupling arises from the interaction terms $\mathbf{f}^\Gamma$ and $\mathbf{F}^j$. Because the effects of bilayer bending, cytoskeleton stretching and

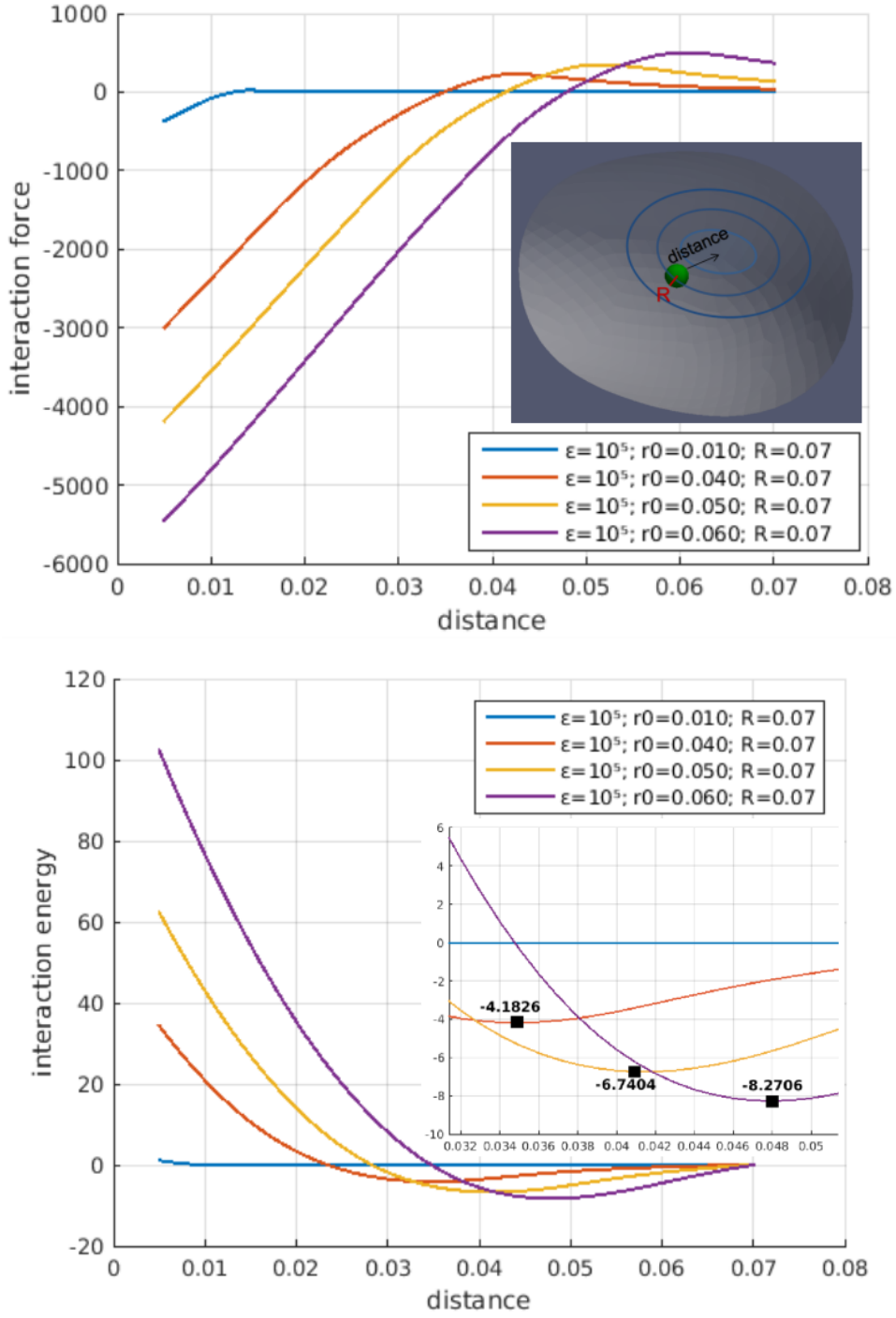

Figure 2. Interaction force $\mathbf{F}$ and energy $\mathcal{E}_{XY}$ induced by $\widetilde{\mathcal{G}}(d, r_0, \varepsilon)$, with $\alpha = 0.89$ and $k = 6$.

surface-to-surface adhesion are derived from energy functions ($\mathcal{E}_Y$, $\mathcal{E}_X$ and $\mathcal{E}_{XY}$, respectively) and the additional forces are dissipative, we automatically have a bound for the total energy

$$\frac{d}{dt}\left(\mathcal{E}_X + \mathcal{E}_Y + \mathcal{E}_{XY}\right) \leq 0 \ . \tag{23}$$

The model equations are certainly too involved to attempt analytical treatment, so that they are discussed through numerical simulations in what follows.

3. Numerical simulations

While the model for the cytoskeleton is discrete by definition, the model for the bilayer is continuous and needs to be discretized. We consider triangulated surfaces in 3D space as approximations for $\Gamma(t)$, which for a fixed mesh connectivity are uniquely described by the vector $\mathbf{Y}$ of vertex positions. Time is discretized so that a sequence of triangulated surfaces $\Gamma^0, \Gamma^1, \dots, \Gamma^n, \dots$ are computed, corresponding to vertex positions $\mathbf{Y}^0, \mathbf{Y}^0, \dots, \mathbf{Y}^n, \dots$. Following Rodrigues et al. [16], on each Γ^n we define the piecewise-affine finite element space $P_1^n = \{f \in C^0(\Gamma^n) : f|_K \text{ is affine}, \forall K \text{ triangle in } \Gamma^n\}$ and the approximation spaces for velocity, surface and curvature $\boldsymbol{W}_h^n = (P_1^n)^3$, $Q_h^n = P_1^n$, $\boldsymbol{K}_h^n = (P_1^n)^3$. We define $\Delta t = t_{n+1} - t_n$ and we update the nodal positions in a Lagrangian way, specifically,

$$\mathbf{X}^{j,n+1} = \mathbf{X}^{j,n} + \mathbf{U}^{j,n+1}\delta t, \quad \mathbf{Y}^{j,n+1} = \mathbf{Y}^{j,n} + \mathbf{w}^{j,n+1}\delta t. \tag{24}$$

With these choices, a fully discrete semi-implicit formulation of the bilayer can be built [16] and coupled to a fully implicit time discretization of (15). At each time step, a nonlinear system of equations is thus built with unknowns $(\mathbf{w}_h^{n+1}, \sigma_h^{n+1}, \boldsymbol{\kappa}_h^{n+1}, p^{n+1}, \mathbf{U}^{n+1}) \in \mathbf{W}_h^n \times Q_h^n \times \mathbf{K}_h^n \times \mathbb{R} \times \mathbb{R}^{3N_X}$ and solved by Newton's iterative procedure. Notice that the formulation is semi-implicit in that the bilayer mesh Γ^n is kept frozen throughout the iterations.

The first simulation we present here to provide insight into the behavior of the 2C-RBC-M consists of the interaction of the bilayer surface with a single cytoskeleton sphere. If the contact energy is weak (ε small) the sphere simply adheres to the bilayer without further effects. However, as ε is increased and becomes comparable to $\varepsilon_1 = \frac{C_{ch}}{R^2 r_0^2}$, the adhesion forces become strong enough to locally deform the bilayer towards wrapping around the sphere. To illustrate this we have considered a single sphere of radius $R = 0.8$, with a contact length scale $r_0 = 0.1$. These values imply $\varepsilon_1 \simeq 3000$. The bilayer initially has a biconcave shape with dimensions 7.8, 7.8 and 2.2 along the x, y and z directions, respectively. We situate the sphere inside the bilayer at a distance $\approx r_0$ and simulate the relaxation of the system for several values of ε between 1000 and 9000. The complete setup and some quantitative results of the attained equilibrium are listed in the Table 1. In Figure 3 we display the different equilibrium shapes of the bilayer colored according to the mean curvature. For $\varepsilon = 1000$ (and smaller) the perturbation in the bilayer shape caused by the sphere is very small. For $\varepsilon = 3000$ and larger the bilayer tends to wrap around the sphere, with its global shape deforming so as to attain an equilibrium under these conditions.

Table 1. Parameters setup and numerical solutions at the equilibrium of the virtual experiment of adhesion between the bilayer and one internal spherical node.

ε	k	R	r_0	c_{CH}	$\mathcal{E}_{\mathcal{Y}}^{\infty}$	$\mathcal{E}_{\mathcal{XY}}^{\infty}$	p	σ
1000	6	0.8	0.1	20	9.08×10^2	-2.20×10^2	-10.6	-1.40×10^3
3000	6	0.8	0.1	20	9.51×10^2	-1.16×10^3	-9.5	-1.50×10^3
5000	6	0.8	0.1	20	1.01×10^3	-2.60×10^3	-8.5	-1.60×10^3
7000	6	0.8	0.1	20	1.07×10^3	-3.90×10^3	-7.5	-1.70×10^3
9000	6	0.8	0.1	20	1.13×10^3	-5.50×10^3	-6.0	-1.80×10^3

Such studies are interesting in relation to the bilayer's reaction to exogenous bodies. A possible application concerns the modeling of the process of invasion of merozoites in the malaria disease, as shown by recent works [39] and [40]. Figure 4 shows how the appropriate use of the interaction force between the lipid bilayer and an external body can be suitable in such applications. On the top-left of the Figure we show microscopy images during the infection process, taken from the work of Riglar et al. [41], while below we show selected snapshots of simulations performed with the 2C-RBC-M. In such applications the transient solution takes on particular interest and the proposed model allows to study the evolution of otherwise inaccessible physical quantities, as shown on the right panel of the Figure 4.

We now turn to study configurations more akin to the RBC membrane, involving the interaction of the bilayer with many connected solid bodies so as to mimic the cytoskeleton component of the RBC. The bilayer is energetically unable to locally deform so as to wrap around the nanometric cytoskeleton nodes. However, since the nodes are elastically connected, their combined action can indeed affect the

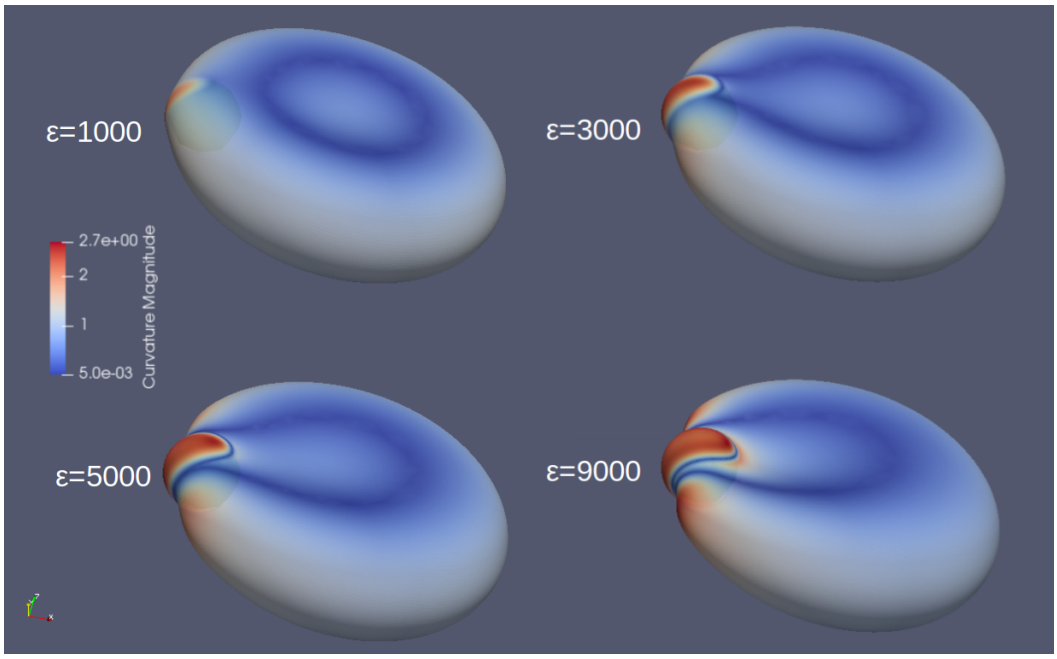

Figure 3. Screenshots of the simulation of one ball ($R = 0.8$) for different values of ε of the RBC in the relaxation process at the equilibrium.

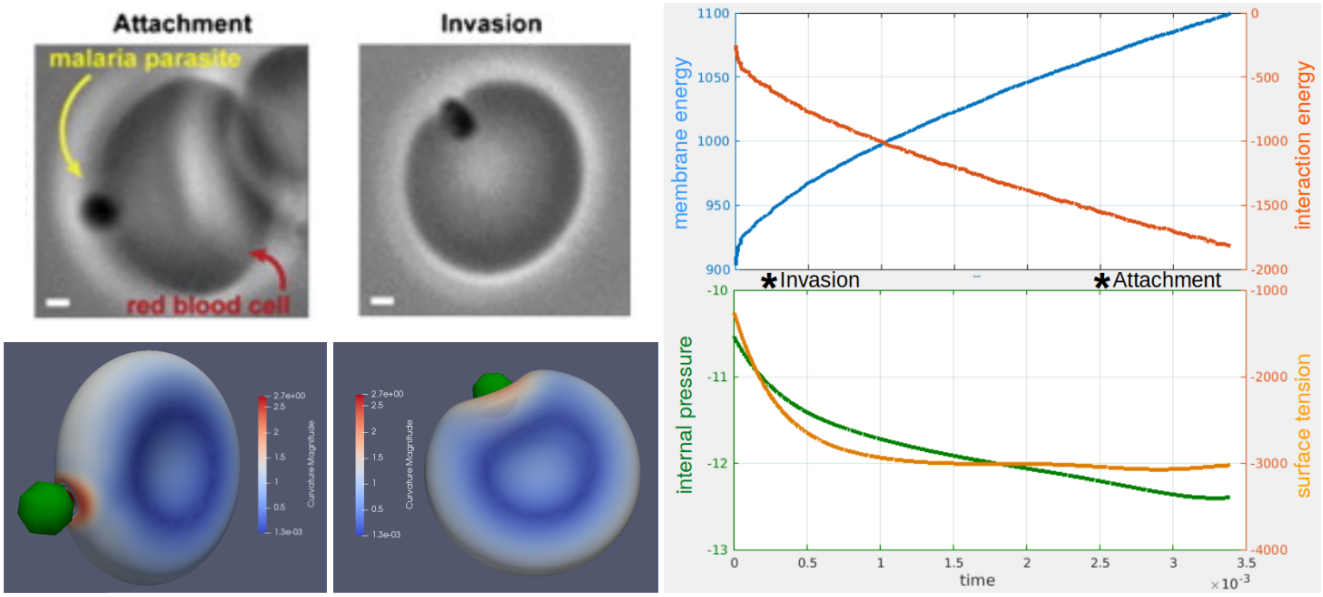

Figure 4. Simplified simulation of the invasion of merozoite in malaria disease performed with the proposed model. Microscopy images taken from [41].

global behavior of the bilayer. We assess the ability of the 2C-RBC-M to relax towards equilibrium from an initial arbitrary shape maintaining the bilayer and cytoskeleton components attached. It is known that RBCs are able to return undamaged to their original shape after substantial deformations, such as those undergone inside the capillaries [42]. There is no doubt that a close relationship exists between the shape of the bio-membranes and their curvature and line tension [43], as well the minimum energy of bending can be consider a possible explanation of the biconcave shape of the human RBC [20]. Moreover, the equilibrium configurations of the bilayer (alone) depend on its reduced volume, defined as $v_r = \frac{6\sqrt{\pi}V}{A^{3/2}}$, being A and V the surface area and internal volume, respectively [44]. The typical RBC has $v_r \approx 0.65$,

so that we select as initial condition an oblate ellipsoid with the same v_r.

Following previous coarse-graining studies [31,45], we set a simplified cytoskeleton with 350 nodes and discretized the bilayer with a triangulation with 10^4 nodes. For the time discretization we adopted a variable time step Δt in the range $[10^{-7}, 10^{-5}]$. Notice that the time unit is $\mu L^2/(k_B T)$, which with $L = 1\,\mu$m and $\mu \approx 10^{-8}$ Pa-s-m can be estimated as ≈ 2 seconds. Unless otherwise specified, the setup of parameters of the following simulations is reported in Table 2. Concerning the interaction parameters, it is possible to estimate the adhesion energy of N spheres that do not deform the lipid bilayer locally as $\approx 2\,\pi^2\,\varepsilon\,r_0^3\,R\,N$. The value of $\varepsilon = 5000$ was chosen such that the adhesion energy is ≈ 400 and thus comparable to the bilayer bending energy. This makes the adhesion to be strong enough for the cytoskeleton to be able to deform the bilayer by pulling from it without detaching. Other necessary data are the persistence length ℓ_p and the constant k_p, which we adjust so that the relaxed length of each cytoskeleton fiber is equal to its length in the initial configuration.

Table 2. Setup of parameters of the relaxation process simulations.

Value	Symbol	Description	Model
1.0	$k_B\,T$	Energy unit	(WLC)
2	n	POW exponent	(WLC)
1.0	β_Γ	Bilayer interaction constant	(INT)
1.0	β_Υ	Cyto interaction constant	(INT)
6	k	Coefficient Lennard-Jones potential	(INT)
5000	ε	Interaction strength constant	(INT)
0.05	r_0	equilibirum cyto-membrane surface distance	(INT)
0.1	R	Radius of cyto-sphere	(INT)
1.0	μ	Viscosity	(BIL)
20.0	C_{ch}	Canham constant	(BIL)
117.5	A_0	Initial RBC surface area	(BIL)
79.6	V_0	Initial RBC volume	(BIL)

The initial bilayer shape is thus taken as an ellipsoid with lengths 8, 8, and 2.4 along the x, y, and z axis, respectively. The initial positions of the cytoskeleton nodes lie at a distance $\approx r_0$ from it. In Figure 5 we show the evolution of the RBC model with and without the cytoskeleton. Also plotted is the total energy as a function of time, which in the case with cytoskeleton contains the contributions of $\mathcal{E}_X$ and $\mathcal{E}_{XY}$. In both cases the model relaxes to a quite realistic biconcave shape at $t \approx 10^{-3}$, with a monotonous decay of the total energy. The full model has a sudden decrease of energy at the first instants, corresponding to the adjustment of the distances between the junctions and the bilayer. The relaxed shapes are shown in the figure colored with the local mean curvature. They are very similar, but in the one corresponding to the full model the small local effect of each cytoskeleton node on the adjacent bilayer is clearly visible. Notice that in this case $\varepsilon = 5000 \ll \varepsilon_1 \approx 8 \times 10^5$, so that it is not expected that the bilayer will significantly tend to wrap around the cytoskeleton nodes.

Table 3. Quantities of numerical solutions at the equilibrium of the relaxation experiment of one-component (without cytoskeleton) and full RBC two-component model.

Case	$\mathcal{E}^\infty$	$\mathcal{E}^\infty_\mathcal{Y}$	$\mathcal{E}^\infty_\mathcal{X}$	$\mathcal{E}^\infty_{\mathcal{X}\mathcal{Y}}$	p	$\overline{\sigma}$
One-component	9.0×10^2	9.0×10^2	–	–	-10.6	-12.8×10^2
Two-component	1.9×10^4	9.1×10^2	2.1×10^4	-3.0×10^3	-10.1	-38.2×10^2

Some relevant global quantities at the equilibrium are reported in Table 3. The introduction of the cytoskeleton component does not affect the bending energy significantly, while a considerable decrease in average surface tension and some increase of the internal pressure can be noted. These observations are consistent with the cytoskeleton exerting an average inwards pull on the bilayer at equilibrium. In order to better understand the impact of the presence of the cytoskeleton in the evolution of the whole system we present below a series of virtual experiments that take this equilibrium as initial condition. We perturb this configuration by changing the equilibrium length ℓ_0 of each spectrin fiber by a constant factor. For example, if we set $\ell_{eq} = 0.9\,\ell_0$, it means that each cytoskeleton fiber will tend to contract

Lipid bilayer neglecting cytoskeleton and interaction forces.

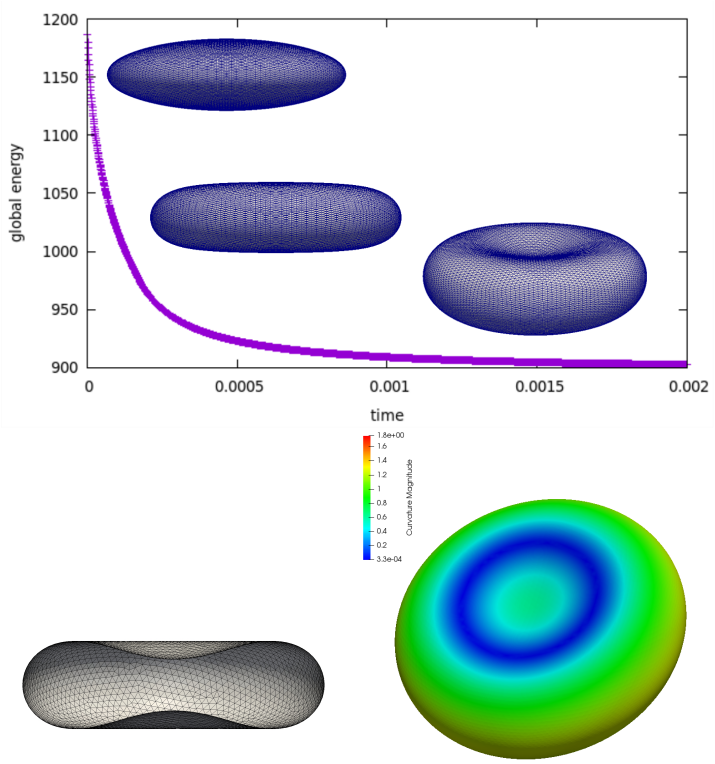

Lipid bilayer considering cytoskeleton and interaction forces.

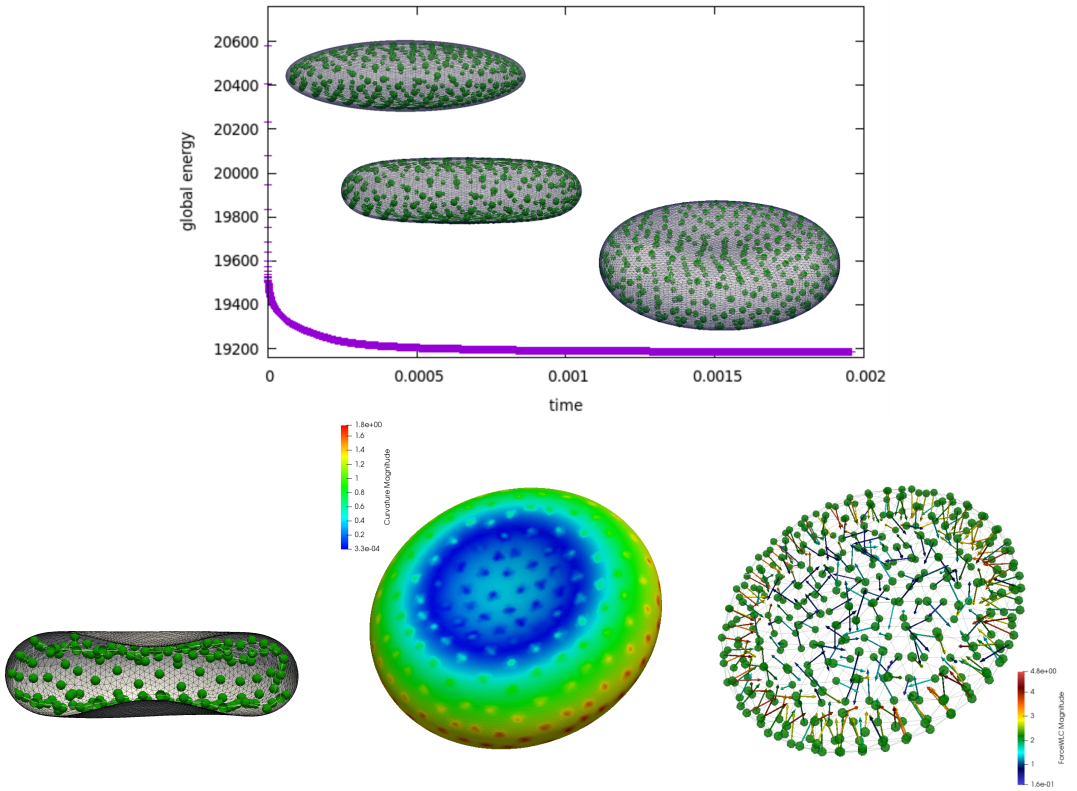

Figure 5. Screenshots of the simulation of the evolution of the RBC in the relaxation process ($t = 0.15$).

towards 90% of its initial length. The execution of this study has highlighted a deformation interval in which, under our hypotheses, the cytoskeleton interacts with the lipid membrane while maintaining its

configuration and attachment to the bilayer.

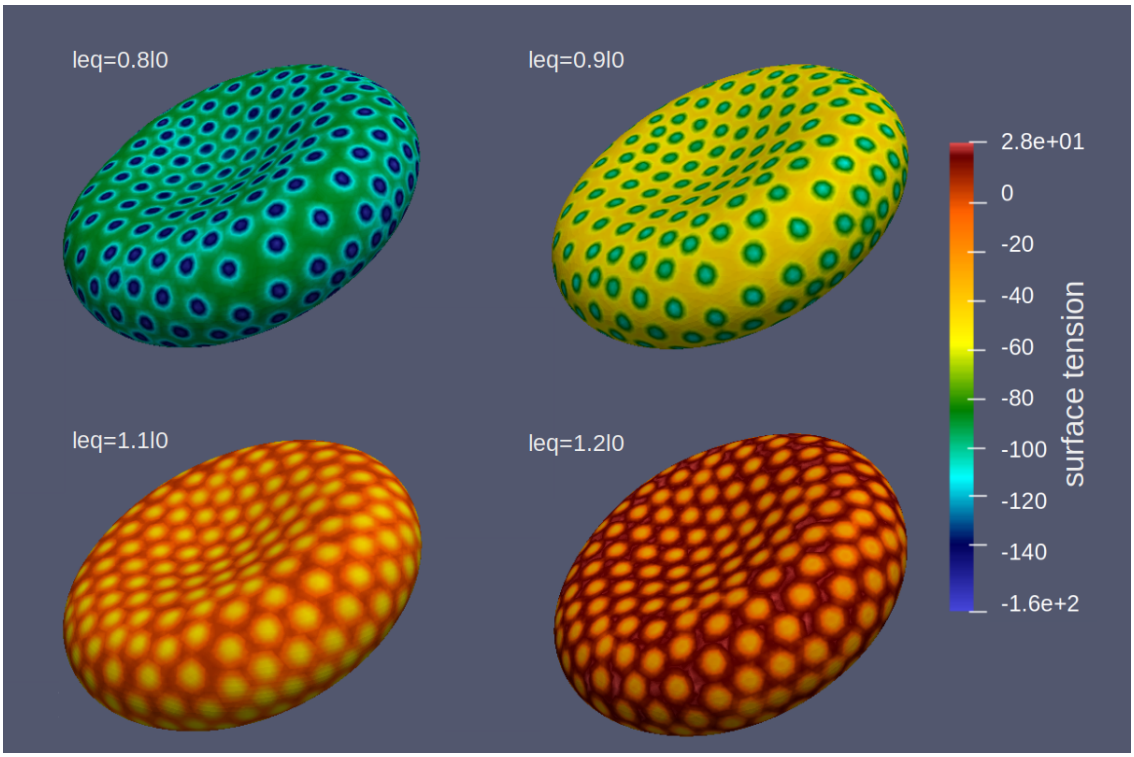

Figure 6. Configuration of the RBC at equilibrium, by contracting and extending the cytoskeleton. The surface tension is displayed with the colors.

Table 4. Global physical quantities corresponding to the steady states reached after different perturbations of the equilibrium lengths of the cytoskeleton fibers.

ℓ_{eq}	$\mathcal{E}^{\infty}$	$\mathcal{E}^{\infty}_{\mathcal{Y}}$	$\mathcal{E}^{\infty}_{\mathcal{X}}$	$\mathcal{E}^{\infty}_{\mathcal{XY}}$	p	$\overline{\sigma}$
$0.8\,\ell_0$	21.26×10^3	9.07×10^2	23.29×10^3	-29.35×10^2	-9.0	-12.5×10^3
$0.9\,\ell_0$	19.88×10^3	9.05×10^2	21.96×10^3	-29.88×10^2	-9.7	-7.2×10^3
$1.0\,\ell_0$	19.30×10^3	9.1×10^2	21.62×10^3	-30.02×10^2	-10.1	-3.8×10^3
$1.1\,\ell_0$	19.77×10^3	9.09×10^2	21.85×10^3	-29.98×10^2	-10.9	-1.4×10^2
$1.2\,\ell_0$	20.34×10^3	9.11×10^2	22.43×10^3	-29.92×10^2	-11.0	5.5×10^1

In Table 4 we list the results of some main quantities corresponding to contraction or extension factors between 80% to 120%. As evident from the cases shown in Figure 6, the average surface tension of the bilayer increases as the cytoskeleton tends to expand. This increase eventually leads to positive surface tension values which could reveal a mechanical-biological reality. As we have previously seen, the one-component model with a fixed reduced volume of the order $v_r \approx 0.65$ leads to a biconcave-shaped membrane with a negative surface tension (see also [46]). Nevertheless there is experimental evidence that the effective surface tension of a RBC is positive and of the order of 10^{-7} J/m^2 [47,48]. In the case $\ell_{eq} = 1.2\,\ell_0$ the execution of our model leads to an average surface tension of comparable value (the scale for σ is $k_B T/L^2 \simeq 4 \times 10^{-9}$ J/m^2. This outcome suggests that the cytoskeletal network exerting an expansive force on the bilayer may reconcile the difference in the sign of the surface tension between theory and experiments. From the screenshots in Figure 6, we can appreciate the local influence of the nodes of the cytoskeleton. Probably this type of influence is excessive and is due to an exaggeration in the weight given to the interaction force (ε can be chosen lower), but it is interesting to validate the model and draw conclusions on the interdependence of the components of the erythrocyte.

We conclude the study by analyzing the extreme cases. If the relaxed length of the spectrin fibers is reduced further, some cytoskeleton nodes detach from the bilayer. In fact, this phenomenon occurs when-

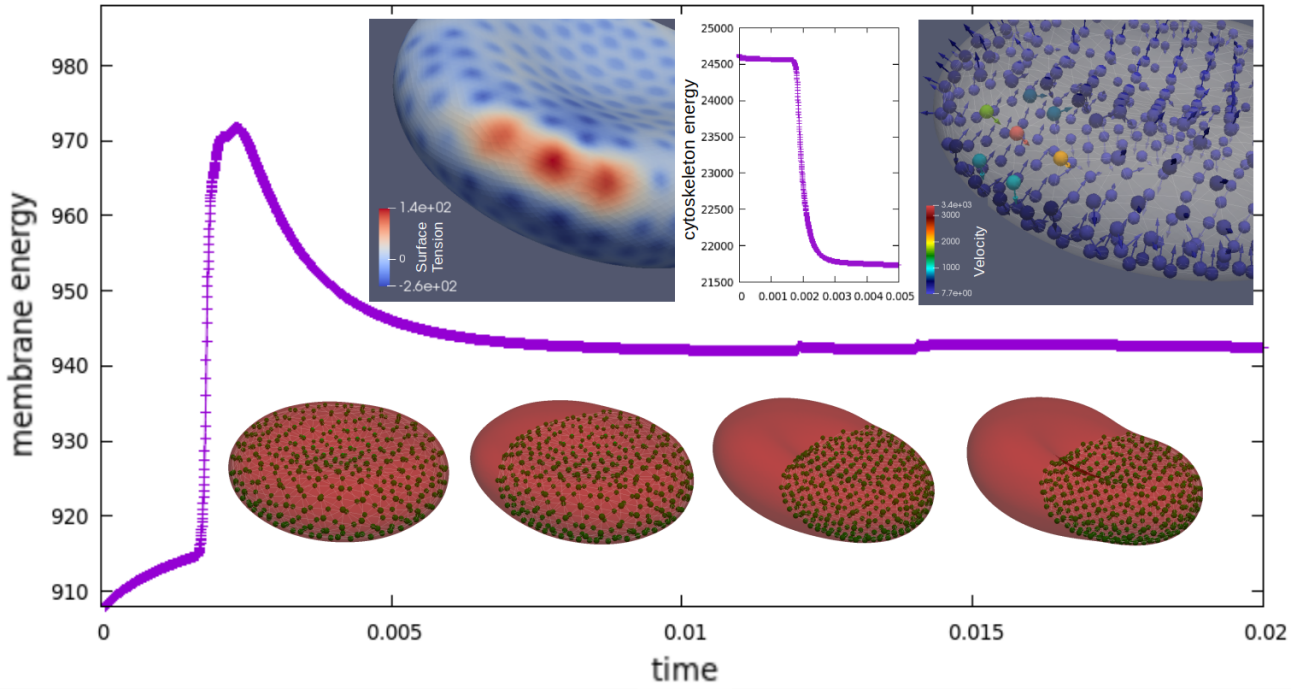

Figure 7. Time evolution of a RBC a $\ell_{eq} = 0.7\,\ell_0$ is imposed, with "detaching" phenomenon of cytoskeleton network.

ever $\ell_{eq} < 0.8\,\ell_0$. In Figure 7 we show the time evolution of a RBC with $\ell_{eq} = 0.7\,\ell_0$, for which detachment of the cytoskeleton starts at $t \approx 0.002$ put into evidence by a sudden increase of the bending energy. In this time interval we can observe the counterpart downward jump of the energy of the cytoskeleton (see graph on top-center). The specific nodes that first detach are shown in the image (on top-right), which also show that the detachment induces a positive local surface tension (see screenshot on top-left). This event is followed by a contraction of the entire network of spectrins which, remaining attached to the a part of the bilayer, contribute to giving the peculiar RBC shape shown in the last screenshot.

The opposite extreme case is when the spectrin network has its equilibrium lengths increased beyond $1.2\ell_0$. We examine in Fig. 8 the numerical results of the simulation imposing $\ell_{eq} = 1.3\,\ell_0$. The compression along the individual spectrins grows while they try to find space for expansion subject to the constraint imposed by the surrounding bilayer. As expected, the spectrin network eventually buckles and locally entangles, as shown in the figure's insert. This event occurs when a series of spectrins of a junctional complex are an over-tension condition compared to the others ones (see the detail on below-left). Notably, this buckling takes place without the nodes detaching from the bilayer. This folding phenomenon leads to a complex evolution of the bilayer energy and results in a perturbation of the biconcave shape of the red blood cell, as shown in the screenshot. This behavior corresponds to an unpredictable and fluctuating trend of the internal pressure (as shown by the graph in the low-center). A final image (on the right) shows the local effect of nodes folding in terms of local surface tension.

4. Conclusions

In this work we have presented a new approach for modeling a single RBC. According to this, we have motivated the need of a new two-component model for a single RBC. We have coupled the established worm-like-chain approach for the cytoskeleton to a continuum model for the lipid bilayer based on a viscous liquid-shell model with Canham-Helfrich bending energy. Another original contribution is represented by the introduction of the adhesion forces modelling the attachment of the cytoskeleton nodes to the bilayer integral proteins. We tested the two-component RBC approach, firstly investigating the interaction of the bilayer surface with a single internal and external body. Then we provided the implementation of the 2C-RBC-M concerning the relaxation of the cell, and comparing it with the

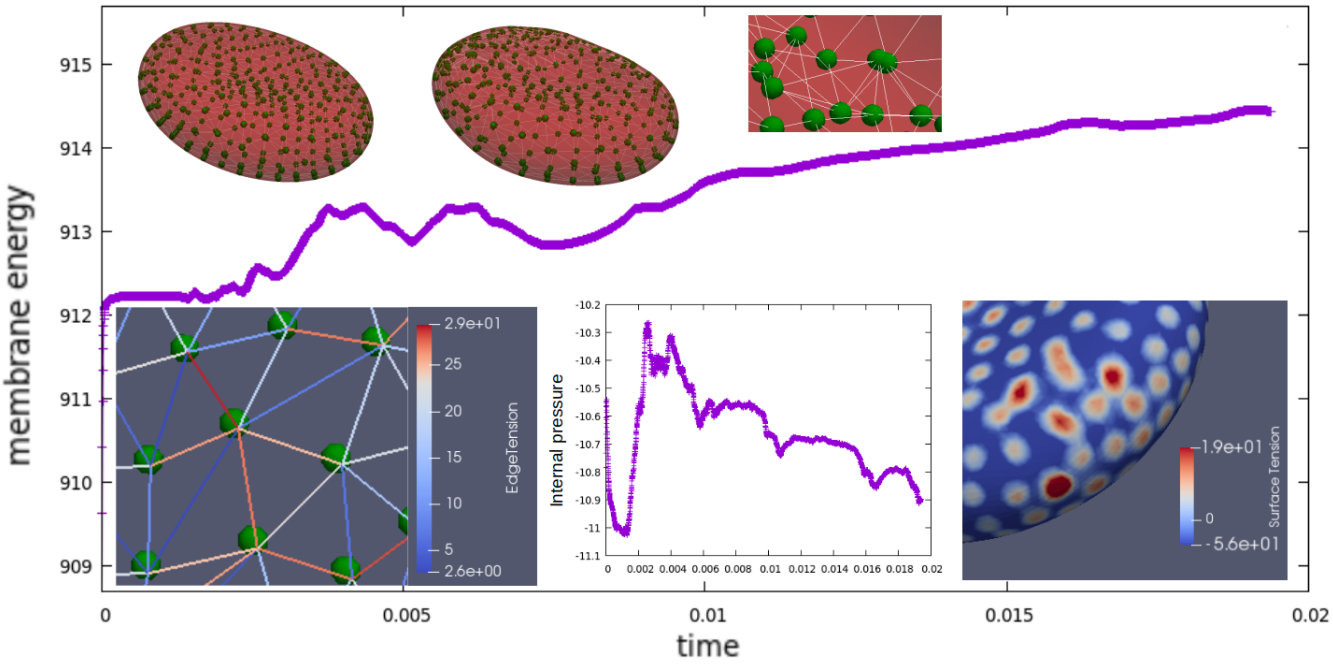

Figure 8. Time evolution of a RBC a $\ell_{eq} = 1.3\,\ell_0$ is applied, with "folding" effect of cytoskeleton network.

one-component model. We have also reported a short study by stressing the bilayer through the perturbation of the cytoskeleton equilibrium state. These virtual experiments not only showed the consistency of the mathematical-computational model but also have suggested physical considerations about the RBC membrane system.

Understanding better the behaviour of a red blood cell means to give a strong contribution to the comprehension of life. Thanks to modern technology, the accuracy of mathematical models can be proven by experimental laboratory tests. Conversely, mathematical modeling can help to identify the reasons behind what is physically observed. Our next goal is to adapt the code in order to simulate the fundamental experiments of micropipette aspiration and optical tweezing. Our deliverable is a software for the "in silico" (or virtual) simulation of RBCs, that extends the range of spatial and temporal scales of current simulators as the OpenRBC code [49] and the implementation in LAMMPS of Fu and co-workers [50].

Acknowledgements

The work was supported by grants from the INCT-MACC (Instituto Nacional de Ciência e Tecnologia - Medicina Assistida por Computação Científica), approved from CNPq (Conselho Nacional de Desenvolvimento Científico e Tecnológico) of Brazil. This research was developed making use of the computational resources (Euler cluster) of the CeMEAI (Center for Mathematical Sciences Applied to Industry) financed by FAPESP (Fundação de Amparo à Pesquisa do Estado de São Paulo) of Brazil (Grant 2013/07375-0). L.M. acknowledges the Foundation CAPES (Coordenação de Aperfeiçoamento de Pessoal de Nível Superior) of the Ministry of Education of Federal Republic of Brazil for economic support (Grant PROEX-9740044/D). G.C.B. acknowledges financial support from FAPESP (Grant 2018/08752-5).

References

1. A. S. Popel and P. C. Johnson, Microcirculation and hemorheology, *Annu. Rev. Fluid Mech.*, vol. 37, pp. 43–69, 2005.
2. G. Mchedlishvili and N. Maeda, Blood flow structure related to red cell flow: determinant of blood fluidity in narrow microvessels, *The Japanese journal of physiology*, vol. 51, no. 1, pp. 19–30, 2001.

3. P. Ulker, L. Sati, C. Celik-Ozenci, H. Meiselman, and O. Baskurt, Mechanical stimulation of nitric oxide synthesizing mechanisms in erythrocytes, *Biorheology*, vol. 46, no. 2, pp. 121–132, 2009.
4. J. Li-Guo, W. Heng-An, Z. Xiao-Zhou, and W. Xiu-Xi, Coarse-grained molecular dynamics simulation of a red blood cell, *Chinese Physics Letters*, vol. 27, no. 2, p. 028704, 2010.
5. M. Ju, S. S. Ye, B. Namgung, S. Cho, H. T. Low, H. L. Leo, and S. Kim, A review of numerical methods for red blood cell flow simulation, *Computer methods in biomechanics and biomedical engineering*, vol. 18, no. 2, pp. 130–140, 2015.
6. A. Fasano and A. Sequeira, *Hemomath: The mathematics of blood*, vol. 18. Springer, 2017.
7. H. A. Svahn and A. van den Berg, Single cells or large populations?, *Lab on a Chip*, vol. 7, no. 5, pp. 544–546, 2007.
8. G. Bao, Y. Bazilevs, J.-H. Chung, P. Decuzzi, H. D. Espinosa, M. Ferrari, H. Gao, S. S. Hossain, T. J. Hughes, R. D. Kamm, *et al.*, Usnctam perspectives on mechanics in medicine, *Journal of The Royal Society Interface*, vol. 11, no. 97, p. 20140301, 2014.
9. D. D. Carlo and L. P. Lee, Dynamic single-cell analysis for quantitative biology, 2006.
10. R. Rodríguez-García, I. López-Montero, M. Mell, G. Egea, N. S. Gov, and F. Monroy, Direct cytoskeleton forces cause membrane softening in red blood cells, *Biophysical journal*, vol. 108, no. 12, pp. 2794–2806, 2015.
11. Z. Peng, X. Li, I. V. Pivkin, M. Dao, G. E. Karniadakis, and S. Suresh, Lipid bilayer and cytoskeletal interactions in a red blood cell, *Proceedings of the National Academy of Sciences*, vol. 110, no. 33, pp. 13356–13361, 2013.
12. X. Li, Z. Peng, H. Lei, M. Dao, and G. E. Karniadakis, Probing red blood cell mechanics, rheology and dynamics with a two-component multi-scale model, *Philosophical Transactions of the Royal Society A: Mathematical, Physical and Engineering Sciences*, vol. 372, no. 2021, p. 20130389, 2014.
13. H.-Y. Chang, X. Li, and G. E. Karniadakis, Modeling of biomechanics and biorheology of red blood cells in type 2 diabetes mellitus, *Biophysical journal*, vol. 113, no. 2, pp. 481–490, 2017.
14. D. A. Fedosov, B. Caswell, and G. E. Karniadakis, Systematic coarse-graining of spectrin-level red blood cell models, *Computer Methods in Applied Mechanics and Engineering*, vol. 199, no. 29-32, pp. 1937–1948, 2010.
15. M. Arroyo, A. DeSimone, and L. Heltai, The role of membrane viscosity in the dynamics of fluid membranes, *arXiv preprint arXiv:1007.4934*, 2010.
16. D. S. Rodrigues, R. F. Ausas, F. Mut, and G. C. Buscaglia, A semi-implicit finite element method for viscous lipid membranes, *Journal of Computational Physics*, vol. 298, pp. 565–584, 2015.
17. R. A. Sauer, Computational contact formulations for soft body adhesion, *Advances in Soft Matter Mechanics*, p. 55, 2012.
18. C. Lanczos, *The variational principles of mechanics, 4th edn.* Toronto University Press, Toronto, 1970.
19. L. Scriven, Dynamics of a fluid interface equation of motion for newtonian surface fluids, *Chemical Engineering Science*, vol. 12, no. 2, pp. 98–108, 1960.
20. P. B. Canham, The minimum energy of bending as a possible explanation of the biconcave shape of the human red blood cell, *Journal of theoretical biology*, vol. 26, no. 1, pp. 61IN777–76IN881, 1970.
21. W. Helfrich, Elastic properties of lipid bilayers: theory and possible experiments, *Zeitschrift für Naturforschung C*, vol. 28, no. 11-12, pp. 693–703, 1973.
22. B. Seguin and E. Fried, Microphysical derivation of the canham–helfrich free-energy density, *Journal of mathematical biology*, vol. 68, no. 3, pp. 647–665, 2014.
23. R. O. Rodrigues, D. Pinho, V. Faustino, and R. Lima, A simple microfluidic device for the deformability assessment of blood cells in a continuous flow, *Biomedical microdevices*, vol. 17, no. 6, p. 108, 2015.
24. R. Löhner, Regridding surface triangulations, *Journal of Computational Physics*, vol. 126, no. 1, pp. 1–10, 1996.

25. A. Bonito, R. H. Nochetto, and M. S. Pauletti, Parametric fem for geometric biomembranes, *Journal of Computational Physics*, vol. 229, no. 9, pp. 3171–3188, 2010.
26. G. Dziuk and C. M. Elliott, Finite elements on evolving surfaces, *IMA journal of numerical analysis*, vol. 27, no. 2, pp. 262–292, 2007.
27. G. Dziuk and C. M. Elliott, Finite element methods for surface pdes, *Acta Numerica*, vol. 22, pp. 289–396, 2013.
28. R. E. Rusu, An algorithm for the elastic flow of surfaces, *Interfaces and Free Boundaries*, vol. 7, no. 3, pp. 229–239, 2005.
29. W. Gratzer, The red cell membrane and its cytoskeleton., *Biochemical Journal*, vol. 198, no. 1, p. 1, 1981.
30. J. Hansen, R. Skalak, S. Chien, and A. Hoger, An elastic network model based on the structure of the red blood cell membrane skeleton, *Biophysical journal*, vol. 70, no. 1, pp. 146–166, 1996.
31. D. Fedosov, B. Caswell, and G. Karniadakis, A multiscale red blood cell model with accurate mechanics, rheology and dynamics, *Biophys. J.*, vol. 98, pp. 2215–2225, 2010.
32. D. A. Fedosov, H. Lei, B. Caswell, S. Suresh, and G. E. Karniadakis, Multiscale modeling of red blood cell mechanics and blood flow in malaria, *PLoS computational biology*, vol. 7, no. 12, p. e1002270, 2011.
33. D. A. Fedosov, B. Caswell, and G. E. Karniadakis, Coarse-grained red blood cell model with accurate mechanical properties, rheology and dynamics, in *2009 Annual International Conference of the IEEE Engineering in Medicine and Biology Society*, pp. 4266–4269, 2009.
34. L. Freund and Y. Lin, The role of binder mobility in spontaneous adhesive contact and implications for cell adhesion, *Journal of the Mechanics and Physics of Solids*, vol. 52, no. 11, pp. 2455–2472, 2004.
35. E. Kuusela and W. Alt, Continuum model of cell adhesion and migration, *Journal of mathematical biology*, vol. 58, no. 1-2, p. 135, 2009.
36. I. Pajic-Lijakovic and M. Milivojevic, Modeling analysis of the lipid bilayer–cytoskeleton coupling in erythrocyte membrane, *Biomechanics and modeling in mechanobiology*, vol. 13, no. 5, pp. 1097–1104, 2014.
37. J. N. Israelachvili, *Intermolecular and surface forces*. Academic press, 2011.
38. L. Meacci, G. C. Buscaglia, R. F. Ausas, and F. Mut, A red blood cell cyto-bilayer interaction model, *Proceeding Series of the Brazilian Society of Computational and Applied Mathematics*, vol. 7, no. 1, 2020.
39. S. Hillringhaus, A. K. Dasanna, G. Gompper, and D. A. Fedosov, Importance of erythrocyte deformability for the alignment of malaria parasite upon invasion, *Biophysical journal*, vol. 117, no. 7, pp. 1202–1214, 2019.
40. S. Hillringhaus, A. K. Dasanna, G. Gompper, and D. Fedosov, Stochastic bond dynamics facilitates alignment of malaria parasite at erythrocyte membrane upon invasion, *bioRxiv*, 2020.
41. D. T. Riglar, D. Richard, D. W. Wilson, M. J. Boyle, C. Dekiwadia, L. Turnbull, F. Angrisano, D. S. Marapana, K. L. Rogers, C. B. Whitchurch, *et al.*, Super-resolution dissection of coordinated events during malaria parasite invasion of the human erythrocyte, *Cell host & microbe*, vol. 9, no. 1, pp. 9–20, 2011.
42. T. M. Fischer, Shape memory of human red blood cells, *Biophysical journal*, vol. 86, no. 5, pp. 3304–3313, 2004.
43. T. Baumgart, S. T. Hess, and W. W. Webb, Imaging coexisting fluid domains in biomembrane models coupling curvature and line tension, *Nature*, vol. 425, no. 6960, p. 821, 2003.
44. U. Seifert, Configurations of fluid membranes and vesicles, *Advances in physics*, vol. 46, no. 1, pp. 13–137, 1997.
45. I. V. Pivkin and G. E. Karniadakis, Accurate coarse-grained modeling of red blood cells, *Physical review letters*, vol. 101, no. 11, p. 118105, 2008.
46. S. K. Veerapaneni, R. Raj, G. Biros, and P. K. Purohit, Analytical and numerical solutions for shapes

of quiescent two-dimensional vesicles, *International Journal of Non-Linear Mechanics*, vol. 44, no. 3, pp. 257–262, 2009.

47. N. Gov, A. Zilman, and S. Safran, Cytoskeleton confinement and tension of red blood cell membranes, *Physical review letters*, vol. 90, no. 22, p. 228101, 2003.
48. T. Betz, M. Lenz, J.-F. Joanny, and C. Sykes, Atp-dependent mechanics of red blood cells, *Proceedings of the National Academy of Sciences*, vol. 106, no. 36, pp. 15320–15325, 2009.
49. Y.-H. Tang, L. Lu, H. Li, C. Evangelinos, L. Grinberg, V. Sachdeva, and G. E. Karniadakis, Openrbc: a fast simulator of red blood cells at protein resolution, *Biophysical journal*, vol. 112, no. 10, pp. 2030–2037, 2017.
50. S.-P. Fu, Z. Peng, H. Yuan, R. Kfoury, and Y.-N. Young, Lennard-jones type pair-potential method for coarse-grained lipid bilayer membrane simulations in lammps, *Computer Physics Communications*, vol. 210, pp. 193–203, 2017.